



From waste to waste: iron blast furnace slag for heavy metal ions removal from aqueous system

Sabah M. Abdelbasir¹ · Mohamed A. Abdel Khalek¹

Received: 14 December 2021 / Accepted: 16 March 2022 / Published online: 31 March 2022
© The Author(s) 2022

Abstract

Inordinate levels of heavy metals in water sources have long been a matter of concern, posing serious environmental and public health risks. Adsorption, on the other hand, is a viable technique for removing heavy metals from water due to its high efficiency, low cost, and ease of operation. Blast furnace slag (BFS) is considered a cheap sorbent for the get rid of Co^{2+} and Pb^{2+} ions from aqueous media. The nonmodified slag is characterized using X-ray diffraction (XRD), X-ray fluorescence (XRF), N_2 adsorption–desorption isotherms, energy dispersive X-ray analysis (EDX), scanning electron microscopy (SEM), and zeta potential. The removal of Co^{2+} and Pb^{2+} ions was carried out using batch adsorption experiments from an aqueous medium. The influence of several variables as pH, contact time, adsorbent dose, temperature, and initial ions concentration was considered. The isotherm, kinetic, thermodynamic, and recyclability were also conducted. The maximum uptake capacity for Co^{2+} and Pb^{2+} was 43.8 and 30.2 mg g^{-1} achieved at pH 6 after 60 min contact time. The adsorption kinetics and isotherms of BFS for Co^{2+} and Pb^{2+} fitted well to Avrami and Freundlich models, respectively. The main adsorption mechanism between BFS and the metal ions was ion exchange. The regeneration of the used slag was studied for reuse many cycles. In terms of economics and scalability, nonmodified BFS treatment has great potential as a cost-effective adsorbent that could be used in water pollution treatment.

Keywords Blast furnace slag · Removal · Adsorption · Heavy metals · Kinetics · Industrial wastewater

Introduction

Noxious heavy metals generated by a variety of manufacturing practices can cause significant environmental harm if not efficiently eliminated from the waste discharges (Sall et al. 2020). These heavy metals adversely affect human health, the environment, and aquatic systems when they accumulate in living creatures at levels above the permitted limits (Fu and Wang 2011; Gupta et al. 2012; Ihsanullah et al. 2016). Among the heavy metal ions, Pb^{2+} and Co^{2+} represent a greater hazard to human health. Acute Pb^{2+} exposure, for example, can result in newborn brain harm as well as nervous system, kidney, and vascular system disorders (Fathy et al. 2021). Generally, when Pb^{2+} ions compile in living

cells, they interact with the proteins' sulfhydryl group disrupting many biological and metabolic activities (Wang et al. 2016). Cobalt noxiousness can induce asthma symptoms as well as liver, thyroid, and heart problems. At high concentrations, it can also cause genetic changes in living creatures (Jaishankar et al. 2014; Sall et al. 2020; Briffa et al. 2020). Furthermore, these two metal ions are recognized as potential cancer-causing agents, and they have been used as model contaminants for adsorption researches despite their toxicity (Khulbe and Matsuura 2018; Abdelbasir et al. 2021).

Eliminating these metals from polluted water is critical for both human health and environmental conservation. Metals are traditionally precipitated by adding hydroxyl or sulfate agents. Nevertheless, those techniques yield significant quantities of hazardous byproducts and are ineffective for negligible metals concentrations (Bazrafshan et al. 2015). For these waters having low metal concentrations, activated carbon adsorption, ion exchange, and membrane technology are effective management options (Alafif et al. 2019). However, the considerable expense and need for pre-treatment are disadvantages of these methods. As a result,

Responsible Editor: Tito Roberto Cadaval Jr

✉ Sabah M. Abdelbasir
sfoda20@hotmail.com

¹ Central Metallurgical Research and Development Institute, P.O. Box 87, Helwan 11421, Cairo, Egypt

a frequently recommended practice for the elimination of heavy metal ions from waste discharges has been the use of economically affordable adsorbents (Saleem et al. 2019). Adsorption process is one of the supreme widely applied methods for wastewater treatment since it is very effective in eliminating pollutants and it is low cost mainly when adding low adsorbent dose (Badawi et al. 2021). There are several sorbent materials that could be utilized for heavy metal adsorption (Abdelbasir et al. 2020; Badawi and Zaher 2021). Such materials comprise, for instance, widely accessible raw materials and wasted industrial byproducts (Nguyen et al. 2018). Natural polymers and zeolites, clay minerals, peat, ash, and slag are the most commonly investigated affordable adsorbents (Carvalho et al. 2011). Notwithstanding its extensive application, the adsorption practice has its own constraints. The most difficult task is the advancement of a sorbent material that is fit for a concurrent and efficient getting rid of contaminants from wastewater at ultra-low levels (Sen Gupta and Bhattacharyya 2014).

Blast furnace slag (BFS) is produced in huge quantities by iron and steel companies, which pose a large major disposal challenge. In 2013, global steel slag output was approximated to be between 170 and 250 million tonnes (Gomes et al. 2018). BFS is a non-metallic output of steel manufacturing. Blast furnaces run at temperatures about 2000 °C and are supplied with regulated mixtures of iron ore ($\text{Fe}_2\text{O}_3 + \text{SiO}_2$), coke (C), and limestone (CaCO_3) and the end products are steel and slag (Medina et al. 2020). Even though the majority of the slag has been disposed of as junk, it has found uses in building and soil improvement. Because BFS is retrieved at high temperatures, the metals present are firmly bound to its matrix and do not easily leach, making it environmentally safe (Kanel et al. 2006). Furthermore, BFS has a high uptake capacity for heavy metals due to the existence of Si and Fe oxides and due to its availability and chemical composition, it can be used as an adsorbent for metals (Liu et al. 2010; Beh et al. 2012; Ahmed and Ahmaruzzaman 2016), phosphate (Xiong et al. 2008; Han et al. 2016), and dyes (Xue et al. 2009; Gao et al. 2017). It can be also used as Fenton-like catalytic agents to break down various organic contaminants (Arzate-Salgado et al. 2016; Nasuha et al. 2016; Cheng et al. 2017). However, several minor components present in steel slag tend to concentrate on the slag surface during crystallization, affecting the adsorption to pollutants. Moreover, due to the limited pore structure of BFS, the internal components are unavailable for utilization efficiently, resulting in a limited adsorption efficiency of the slag. Several researchers have employed various activation and/or conversion technologies to improve the adsorbing performance of BFS. Zhan et al. (2019) employed bentonite-steel slag composite powders as an adsorbent

to treat acid mine drainage containing Pb^{2+} . Chen et al. (2020) prepared acid-modified steel slag as a new type of adsorbent to remove U^{6+} in an aqueous solution. Slag has been converted to calcium silicate hydrate to remove Pb^{2+} , Zn^{2+} , and Cu^{2+} from wastewater (Yang et al. 2019), and to remove Sr^{2+} and Cs^+ (Tsutsumi et al. 2014). To adsorb Co^{2+} ions from aqueous solution, it was also converted into Slag-Oxalate composite (Le et al. 2021). NaOH was used to activate BFS, which was then used to remove Ni^{2+} from aqueous solutions (Sundhararasu et al. 2021). The post-grafting method was used to modify BFS with γ -aminopropyltriethoxysilane (APTES) to improve its adsorption performance (Wang et al. 2021).

Most of the previous works were focused fundamentally on BFS modification or conversion to maximize its chemical and economic potentials. So, the target of our work was to look into the use of BFS, as it is without modification or conversion to other material, for the elimination of cobalt and lead ions from wastewater by adsorption. To evaluate its performance as an adsorbent, batch experiments were carried out and different parameters such as the initial concentration, pH, adsorbent dose, contact time, and temperature were considered. The relating adsorption isotherms, kinetics, and thermodynamics were thoroughly studied. The findings of this study will have a major impact on the use of low-cost adsorbents for wastewater treatment, resulting in reduced waste generation.

Experimental

Materials

A 5 kg sample of iron slag was obtained as a byproduct from the Egyptian Iron and Steel Co., Tabbin, Egypt (29.80° N and 31.31° E). It was firstly rinsed with pure water for surface impurities removal then dried out at 105 °C for a whole night. It was ground and classified according to particle size. The sample was endured to a size reduction by means of a rotating ball mill with nineteen steel balls weighing 540 g each; the longer the grinding time (almost 2 h), the finer and non-agglomerated the particles became.

Nitrate salts of cobalt [$\text{Co}(\text{NO}_3)_2$] and lead [$\text{Pb}(\text{NO}_3)_2$] (pure Sigma-Aldrich and Merck grade) were utilized for the preparation of Co^{2+} and Pb^{2+} stock solutions using ultrapure water. Standard solutions of NaOH and HCl (0.1 mol L⁻¹) were applied for pH monitoring.

Characterization

Chemical composition and full characterization of BFS were determined using different characterization tools (see

Table 1 Chemical composition of blast furnace slag

Element	Na	Zn	Mg	Si	S	K	Ca	Ti	Mn	Fe	Ba	Others
Wt. % as oxide	0.80	0.14	2.93	23.7	2.02	1.02	46.62	1.08	8.88	0.93	11.15	0.73

supplemental file for full details). The chemical composition of the BFS was detected as metal oxides. The concentration of Co^{2+} and Pb^{2+} ions was determined by atomic absorption spectroscopy (GBC-908136 AA, Australia) (Limiju 2017).

Adsorption experiments

The characterized slag was applied as an adsorbent for Co^{2+} and Pb^{2+} ions. Adsorption experimentations were executed using 0.05 g of slag powder in 30 mL of ions solution of desired concentration, temperature, and pH in a 50 mL round bottom bottle. The bottle was shaken in a water bath at 200 rpm for a certain time. Then, the solid adsorbent is removed using a centrifuge. The residual ions were analyzed by atomic absorption spectrophotometer (AAS).

The amount of adsorbed ions per unit weight of slag, q (mg/g), is determined from the following relation (Maged et al. 2020):

$$\text{Adsorption capacity } "q" \text{ (mg/g)} = \frac{(C_i - C_f) \times V}{W} \quad (1)$$

The percent removal of ions was estimated from the following relation (Abdelbasir et al. 2021):

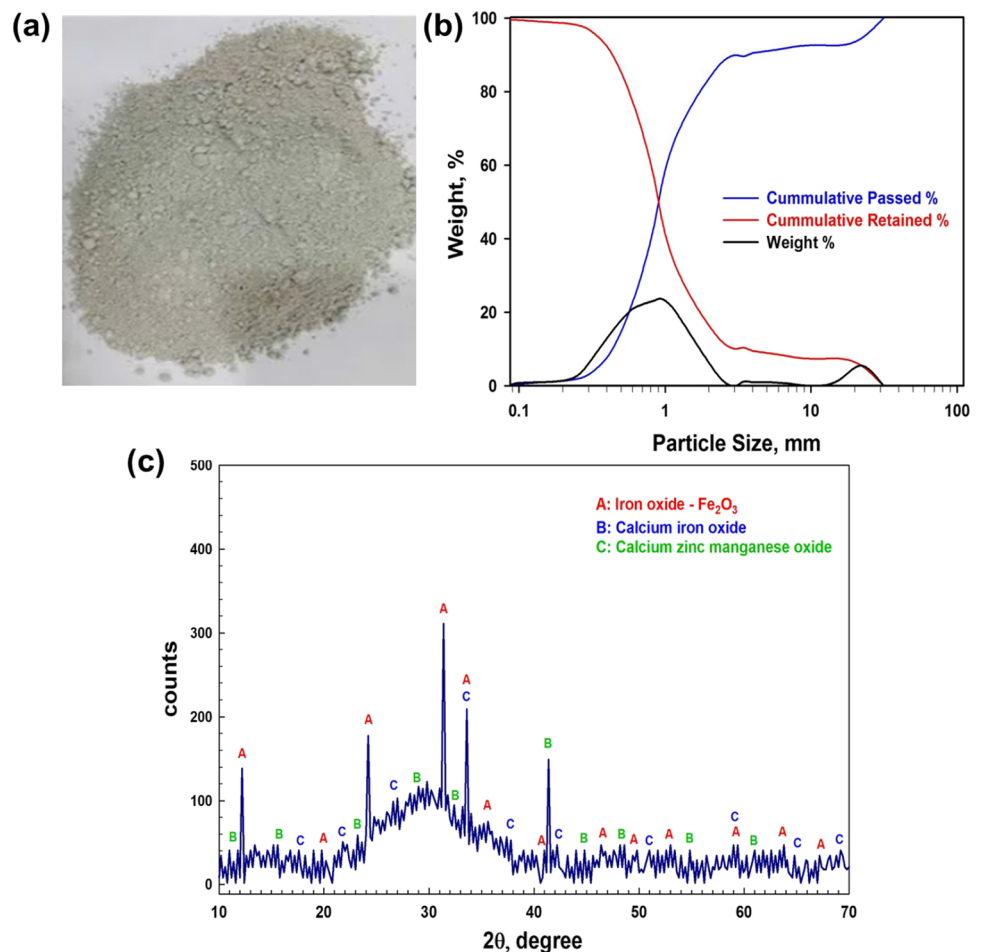
$$\text{Removal efficiency \%} = \frac{C_i - C_f}{C_i} \times 100 \quad (2)$$

Applying that: V is the solution volume in liter (30 mL = 0.03 L), W is the slag dose (g), C_i and C_f are the original and final ions' concentrations (mg L^{-1}).

Regeneration and desorption study

To lower the expenses of the sorption practice and recover the contaminant removed from the waste effluent, the regeneration of the adsorbent is a necessity. A $0.1 \text{ mol L}^{-1} \text{ HNO}_3$ solution was used to study the desorption of the adsorbed

Fig. 1 **a** A photo of the ground BFS, **b** size analysis of the ground sample, weight, cumulative passed and retained, and **c** XRD pattern of BFS



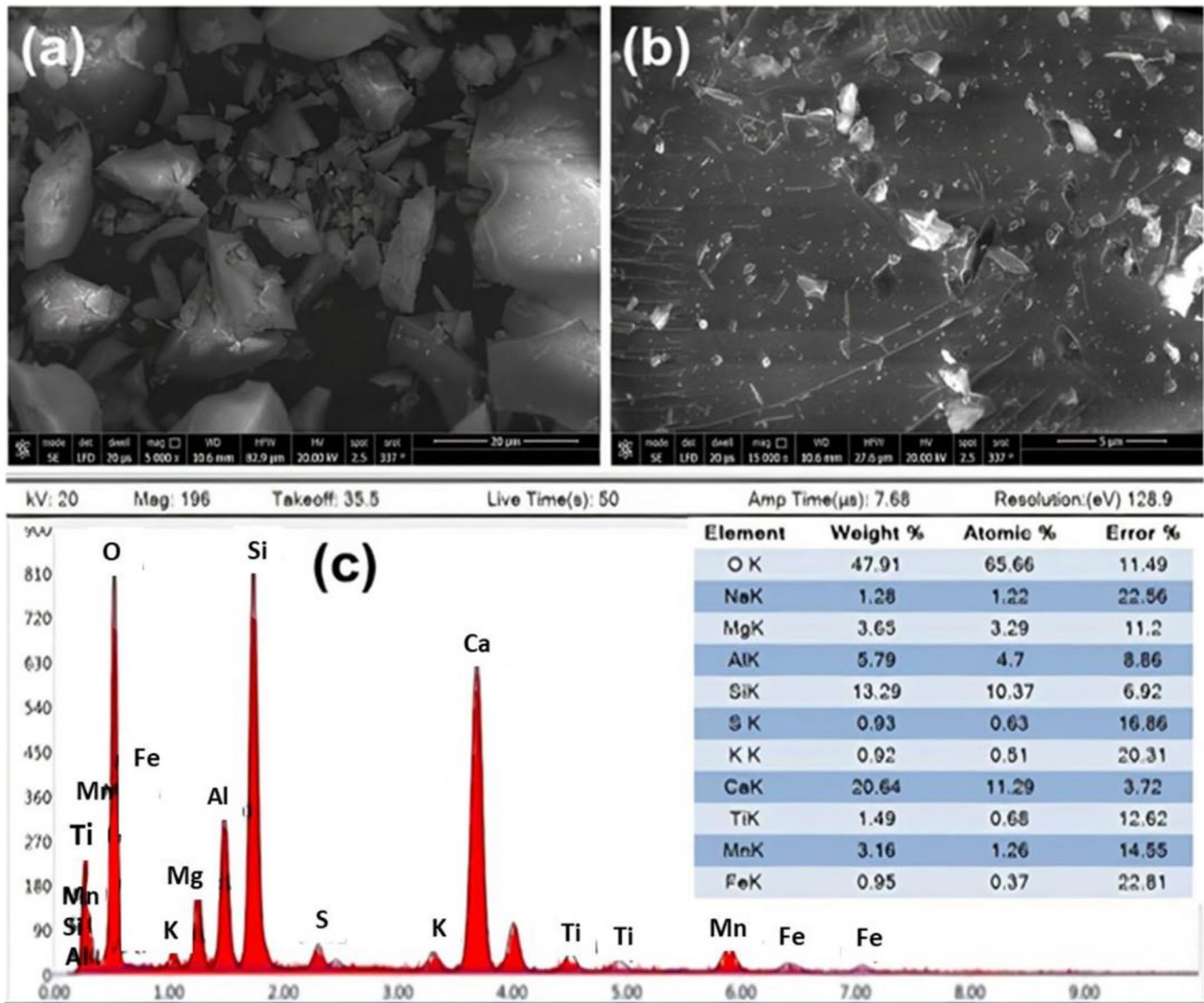


Fig. 2 SEM images: a 20 μm, b 5 μm, and c EDX analysis of BFS

ions at 60 °C for 30 min. (1:10 solid–liquid ratio). Solutions were finally separated from the solids by centrifugation followed by filtration. AAS was used to measure the ions concentration preceding to and following desorption experiments. Equation (3) was used to calculate the desorption efficiency:

$$R_{des} = \frac{D_{des}}{A_{des}} \times 100 \tag{3}$$

The amounts of adsorbed and desorbed metal ions are represented by A_{ads} and D_{des} , correspondingly. Reusability was achieved by utilizing the regenerated adsorbent in subsequent adsorption experiments and repeating the adsorption–desorption method with the same adsorbent sample.

Results and discussion

Slag characterization

The X-ray fluorescence (XRF) analysis of BFS was achieved after grinding and the elemental composition is shown in Table 1. The average content of Ca as oxide (CaO) was approximately 46.62%, as the main element of BFS, followed by Si, Ba, Mn, and Mg. The values represent an average duplicate of BFS analysis. Figure 1a shows a photo of the ground BFS.

The particle size analysis of the slag is shown in Fig. 1b. It is seen that about 50% of the sample has a particle size less than 0.90 mm, while a 90% weight of the sample is less than 0.43 mm. Also, about 80% of the sample has a particle size range of 0.417–1.16 mm. The degree to which finer particles

are reduced is widely known to be subordinate to the material type, the mill, and the grinding circumstances (Petraakis and Komnitsas 2019).

Figure 1c depicts the X-ray diffraction (XRD) pattern of BFS. The pattern is quite intricate which is mostly due to the raw material nature. The sample is possibly amorphous glassy having a hump at about $2\theta:28^{\circ}$ – 33° (Mostafa et al. 2001). It is also worth mentioning that quite a few peaks were found indicating the presence of crystal phases in the slag.

SEM and energy-dispersive X-ray (EDX) analyses were utilized to define the size and basic structure of the BFS as displayed in Fig. 2. SEM images revealed the coarse, slack, and porous surface textures of the BFS sample (Fig. 2a and b). Slag particles had become angular in form, with definite asperities and edges evident. Rough surface textures were also a feature of them. The EDX analysis revealed high-intensity peaks for Ca, O, Si, Al, Mg, and other noticeable ones for Na, Ti, and S, in conformity with the analysis and XRD outcomes. Steel slags are known to include oxides, which are produced during the steelmaking process.

CaO is the most common oxide found in steel slags generated during diverse steelmaking processes (Yildirim and Prezzi 2011). In our case, FeO is another oxide generated during some steelmaking practices with a low occurrence. Slag leachates are also frequently found to be extremely basic because of CaO and further basic oxides (Riley and Mayes 2015).

The surface area and the pore structure of BFS were assessed by the nitrogen isotherms analysis shown in Fig. 3a. As we can see from the figure, the shape of the isotherm is classified as Type II, indicating that the slag with

a heterogeneous granular aspect established the slit aperture shaped by the particles' accumulation (Deng et al. 2020). The specific surface, pore-volume, and average diameter of BFS are revealed in Table S1 in the supplemental file.

Figure 3b shows the surface charge results of the slag in an electrolyte solution. The slag surface charge is clearly pH-dependent, being positively charged at pH less than 4.8, and becoming negatively charged as the solution pH progressed to neutral and basic regions. A pH 4.8 was found to be the isoelectric point (IEP).

Adsorption experiments

Adsorption batch experimentations were applied to validate the heavy metal removal efficiency using BFS as adsorbent for Pb^{2+} and Co^{2+} ions from the prepared solutions.

Impact of pH

The sorption procedure is greatly impacted by the medium's pH. Figure 4a shows the removal efficiency and uptake capacity of different ions from synthetic solution. The maximum sorption capacities and removal efficiency are accomplished at pH 6. Metal ions solubility reduces at alkaline pH, enabling precipitation and complicating sorption (He et al. 2015). The concentration of external H^+ rose at low pH levels which are considered as competitive in ion exchange (Akhigbe et al. 2015; Kozera-Sucharda et al. 2020). The slag selectivity follows the order of $Co^{2+} > Pb^{2+}$. The charge density (charge/ionic radius), hydration energy, and proportions of the hydrated

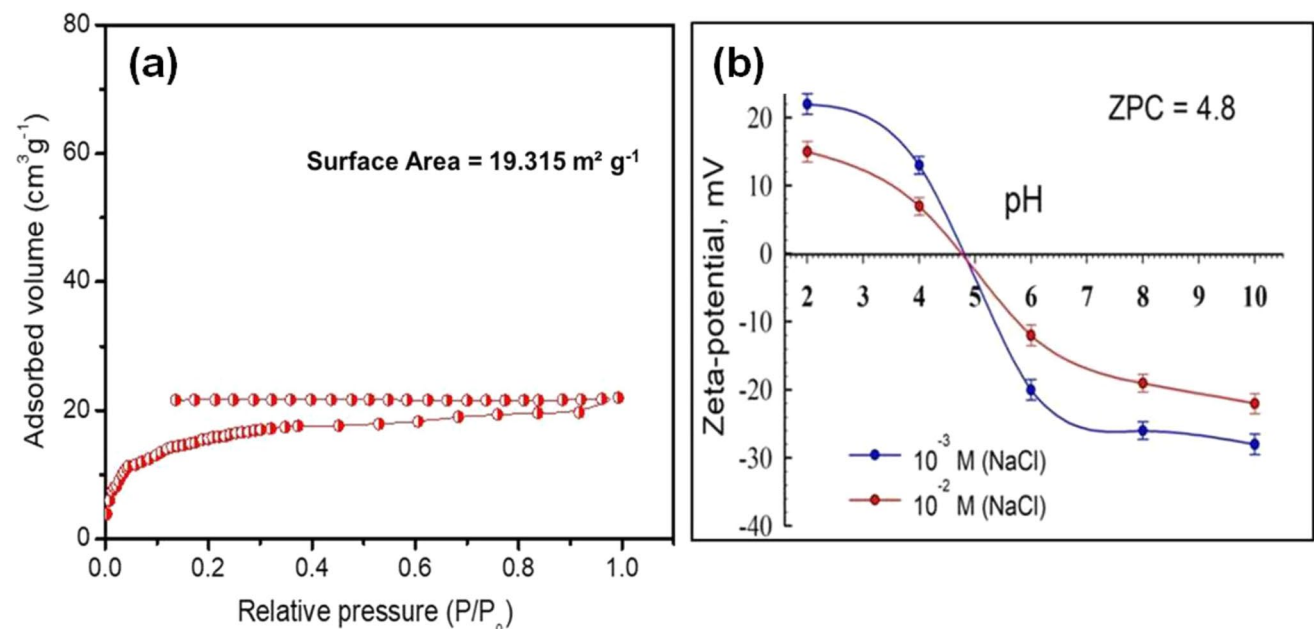


Fig. 3 a N_2 adsorption isotherm and b zeta potential of the BFS

ions may all be used to predict the solid's vantage for various ions all through competitive sorption (see Table S2 in the supplementary file). Other factors, such as the geometry and/or orientation of the ions, also influence selectivity. As well, the distribution of the surface charge on slag can change based on its composition and activation. As a result, solution pH has a significant impact on the adsorbent's functional group activity. The slag surface charge is negative at a pH higher than 4.8 (Dimirkou 2007; Acheampong et al. 2010; Elboughdiri 2020). The distinct ability to adsorb ions is due to the slag's containment (Wang et al. 2021).

Impact of sorbent dosage

Figure 4b validates the action of the slag dose (g L^{-1}) on the elimination efficiency and uptake capability of the slag. The amount of added slag to the aqueous solution significantly affects the adsorption process. Intensifying the dose caused an upsurge of the removal efficiency while the adsorption capacity was increased up to 1.67 g L^{-1} , and then decreased. Each metal ion is subjected to a larger unit mass of the adsorbent, which has more adsorption sites which ready to attract this ion (Mahmoud et al. 2019).

Impact of original metal ion concentrations and sorption isotherms

Figure 5 exhibits the initial ion concentration's influence on the removal efficacy and uptake capacity of the slag. The concentration of ions in an aqueous medium significantly affects the adsorption practice (Abdel-Khalek et al. 2017). Increasing the initial ion concentration increased

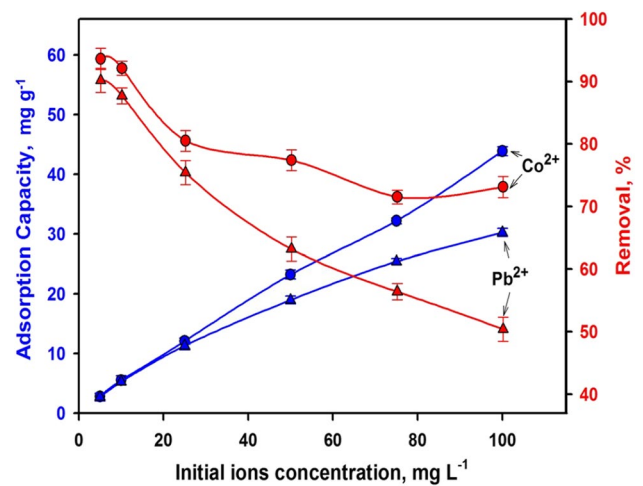


Fig. 5 Effect of initial concentration on the removal efficiency and adsorption capacity (adsorbent dose: 1.67 g L^{-1} , contact time: 60 min, at solution pH: 6 and room temperature)

the uptake capacity and removal efficiency. A high starting concentration indicates that more ions are accessible and hence, more ions are sorbed for a fixed sorbent's amount (Khalek et al. 2019). At a higher initial concentration, the driving forces to conquer the mass transfer barrier for ions' emigration through the medium to the sorbent solid surface upsurgers. Nevertheless, each unit weight of the sorbent is exposed to a greater amount of ions steadily loading the sites until fullness (Mahmoud et al. 2019).

The adsorption isotherms are the best analysis method to describe the sorption behavior (Hałas et al. 2017). Temkin, Langmuir, and Freundlich isotherms were employed to investigate the sorption practice.

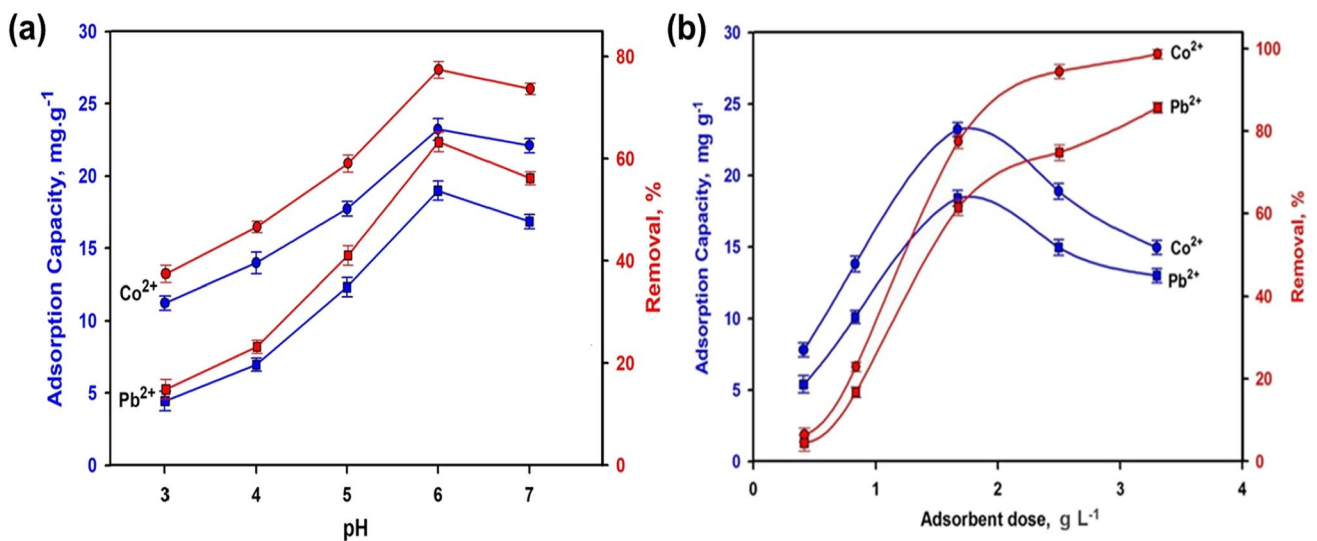


Fig. 4 **a** Effect of pH (initial concentration: 50 mg L^{-1} , adsorbent dose: 1.67 g L^{-1} , contact time: 60 min at room temperature). **b** Effect of slag dose (initial concentration: 50 mg L^{-1} , contact time: 60 min at room temperature) on the removal efficiency and adsorption capacity of slag

Temkin isotherm

According to the Temkin model, the adsorption heat of sorbed species in the layer declines linearly rather than logarithmically as a function of temperature (Ostrovskii 1989; Ho and McKay 1998; Hoslett et al. 2020). Temkin model equation is written as (Tsai and Chen 2013):

$$q_e = B \ln A_T + B \ln C_e \quad (4)$$

where q_e is the adsorbed ions at equilibrium, A_T is the equilibrium constant interrelated to the maximal binding energy ($L g^{-1}$), B is the Temkin isotherm constant linked to the heat of adsorption (J/mol), R is the universal gas constant ($8.314 J/mol/K$), and T is the temperature in kelvin. By plotting q_t against $\ln C_e$, the constants were assessed from the

plot intercept and slope (Fig. 6). A_T and B values are found in Table 2 (the computed R^2 values are 0.8476 and 0.8914).

Langmuir isotherm

Langmuir model's equation (Chen et al. 2012) is:

$$\frac{C_f}{q_t} = \frac{C_f}{q_{\max}} + \frac{1}{b q_{\max}} \quad (5)$$

Knowing that C_f ($mg L^{-1}$) is the final ions concentration, q_t ($mg g^{-1}$) is the adsorbed ions' amount at time t , q_{\max} ($mg g^{-1}$) (highest sorption) is monolayer sorption capacity, and b ($L mg^{-1}$) is a constant associated with the sorption energy. Langmuir model adopts that the occurrence of sorption at a precise homogeneous surface of

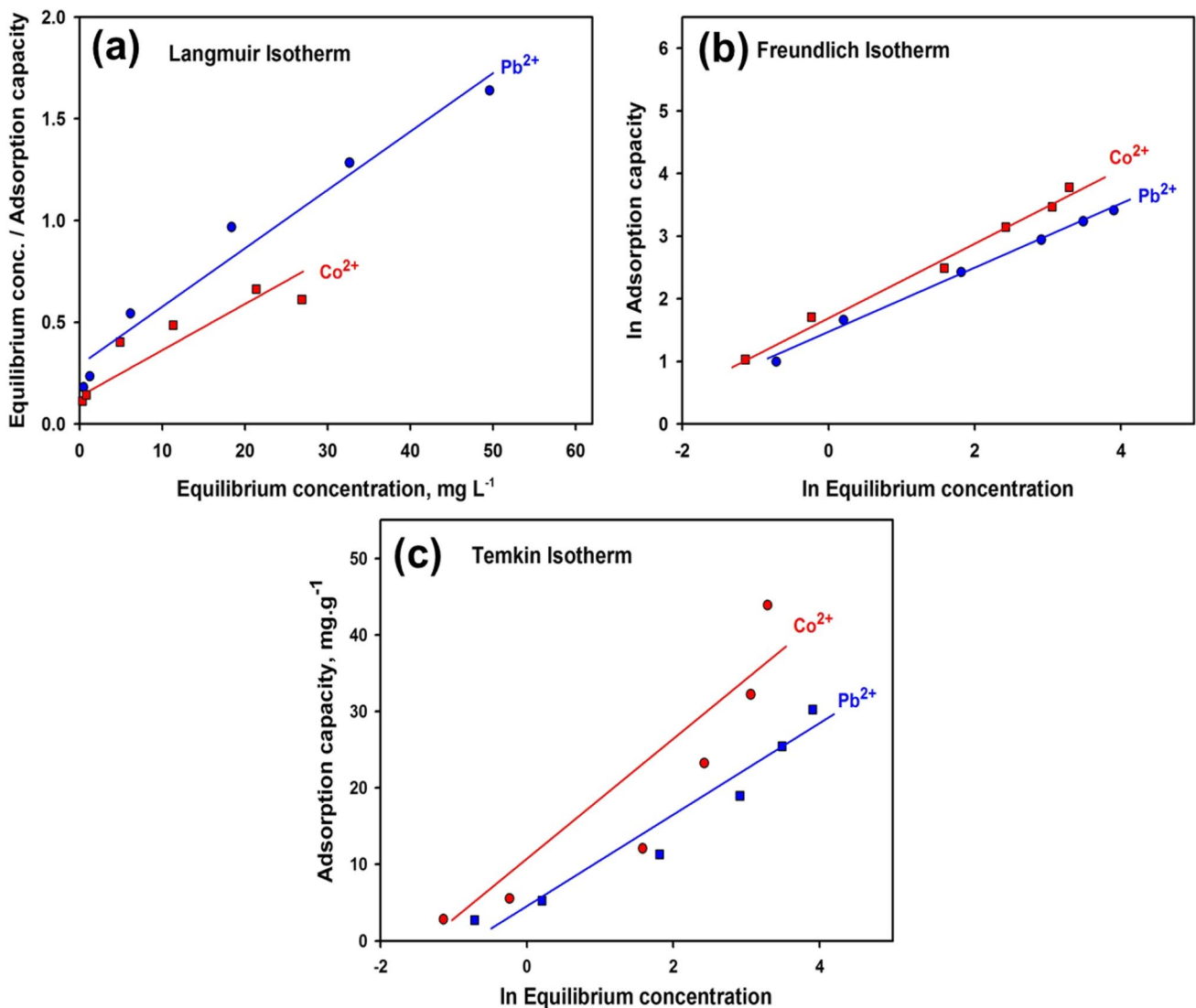


Fig. 6 Plotting results according to **a** Langmuir, **b** Freundlich, and **c** Temkin isotherms ((initial concentration: $50 mg L^{-1}$, contact time: 60 min at room temperature)

Table 2 Parameters of Temkin, Langmuir, and Freundlich isotherm models for the slag

Isotherm	Parameter	Pb ²⁺	Co ²⁺
Temkin	<i>R</i> ²	0.8914	0.8476
	<i>B</i>	5.7920	8.1673
	<i>A_T</i> (L/g)	2.1557	2.5745
	RMSE	9.3838	12.3143
Langmuir	<i>R</i> ²	0.9655	0.8372
	<i>b</i> (L/mg)	0.1062	0.0986
	<i>q_{max}</i> (Cal.)	34.0	52.1
	<i>q_{max}</i> (Exp.)	30.2	43.8
	RMSE	2.1254	12.3154
Freundlich	<i>R</i> ²	0.9950	0.9895
	<i>n</i>	1.958	1.707
	<i>K_f</i> (mg/g)	4.293	5.631
	RMSE	0.5492	0.6731

the adsorbent where the ions flow through the pores and the apertures of the lattice to replenish the substitutable ions of the sorbent. From Fig. 6 and Table 3, the regression (*R*²) value of Langmuir model linear fitting 0.8372 and 0.9655.

Freundlich isotherm

This isotherm model (Visa 2016) equation could be written as:

$$\ln q_t = \ln K_f + \frac{1}{n} \ln C_f \tag{6}$$

where *K_f* (Freundlich constant, mg/g) is the connotative of the degree of the sorption and *n* is the sorption intensity.

K_f points to the uptake capacity, whereas *1/n* is a function of the sorption capability (Tsai and Chen 2013; Shehab et al. 2019). If *n* = 1, the barrier between the two phases is unaffected by concentration. If *n* is less than 1, it assigns typical adsorption and if it lies between 1 and 10, a favorable sorption process is nominated (Goldberg 2018). From Table 2, the

Table 3 The dimensionless separation factor or equilibrium parameter (*R_L*)

Initial conc., mg L ⁻¹	<i>R_L</i>	
	Pb ²⁺	Co ²⁺
5	0.9888	0.9896
10	0.4850	0.5035
25	0.2736	0.2886
50	0.1585	0.1686
75	0.1115	0.1191
100	0.0861	0.0921

values of *n* are 1.707 and 1.958 while *R*² values are 0.9895 and 0.995, indicating that the sorption procedure is favorable and of physical character (Abdel-Khalek et al. 2020).

The dimensionless equilibrium parameter or separation factor (*R_L*)

It is assigned as:

$$R_L = \frac{1}{(1 + bC_0)} \tag{7}$$

Implying that *C₀* (mg L⁻¹) is the initial metal ions' concentration and *b* is Langmuir's constant. *R_L* value specifies whether the sorption is advantageous or non-advantageous. If *R_L* values lie between 0 and 1 then, the sorption procedure is auspicious, whereas *R_L* = 1 denotes non-advantageous linear sorption, and *R_L* = 0 signifies non-reversible sorption.

The results showed that the value of *R_L* is almost unity with 5 mg L⁻¹ which indicates unfavorable adsorption. While at other concentrations up to 100 mg L⁻¹, *R_L* is between 0 and 1 designating advantageous adsorption.

Time impact and sorption kinetics

To find an appropriate contact time for the adsorption, the uptake capacity and removal efficiency of various ions were evaluated as a function of time (Fig. 7). The equilibrium time was determined to be 60 min. The increased sorption rate at the early 20 min is owing to the accessibility of ions and vacant sorption spots on the slag's surface. Then, the sorption active spots steadily lessened, and the extent of sorption was assessed by the number of ions transferred from the solution to the sorption active spots. Thus, the sorption

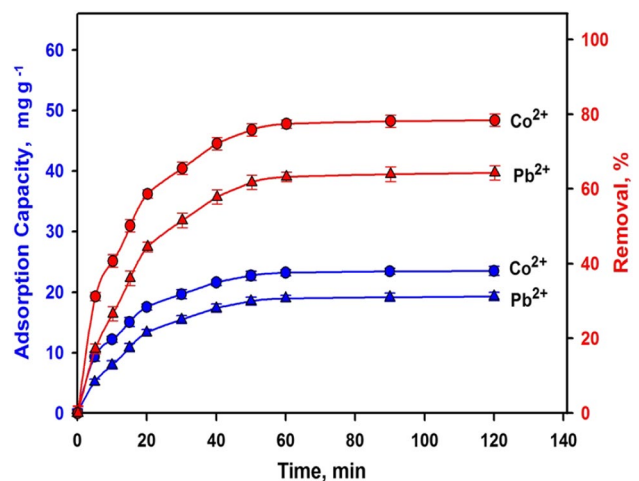


Fig. 7 Effect of conditioning time on the removal efficiency and adsorption capacity of slag (initial concentration: 50 mg L⁻¹, adsorbent doze: 1.67 g⁻¹, solution pH: 6 at room temperature)

increases with time until fullness is reached (Zare et al. 2018; Abdel-Khalek et al. 2020). Also, the ions required more time to penetrate the tiny pores. The higher initial rate implies that the adsorption happens on the exterior surface first, ensued by the interior pores (Nguyen et al. 2018). Furthermore, the larger adsorption amount in the first period demonstrated higher sorption on the exterior surface rather than in the pores (Zare et al. 2016).

The sorption extent of metal ions by the slag was examined via the Lagergren pseudo-first-order and pseudo-second-order models. Also, the Avrami model was used which describes a fractional kinetic order (Lopes et al. 2003; Issaoui et al. 2021). The Lagergren for the pseudo-first-order (PFO) and pseudo-second-order (PSO) models were denoted as shown in the coming equations:

$$\text{PFO model } \ln(q_e - q_t) = \ln q_e - K_1 t \quad (8)$$

$$\text{PSO model } t/q_t = 1/K_2 q_e^2 = t/q_e \quad (9)$$

where k_1 (min^{-1}) and k_2 ($\text{g mg}^{-1} \text{min}^{-1}$) are the equilibrium rate constants.

The Avrami model was expressed as follows (He and Duan 2016; Narayanan et al. 2020):

$$\ln[-\ln(1 - \alpha)] = n \ln K_{avr} + n \ln t \quad (10)$$

The model explains a system with a time-dependent rate coefficient. It provides the greatest fitting of metal ion intake on sorbents (Issaoui et al. 2021; Vaghetti et al. 2009). The integral form is where K is the Avrami constant, and n is a constant interrelated to the sorption mechanism.

$$Q_t = Q_m - Q_m e^{-K_{avr} t^n} \quad (11)$$

$$\frac{Q_t}{Q_m} = 1 - e^{-K_{avr} t^n} \quad (12)$$

The $\frac{Q_t}{Q_m}$ is the adsorption fraction “ α ”. By plotting “ $\ln[-\ln(1 - \alpha)]$ ” versus “ $\ln t$,” the n and K can be computed from the intercept and slope as follow: the slope equal “ n ” and the intercept equals “ $n \ln K$.”

The acquired outcomes of the three linearized models are displayed in Fig. 8; besides, their equivalent limits are listed in Table 4. Even though the PFO and PSO models are the most widely applied that forecast closer values of the equilibrium uptake capacity, the best-fitting was found using Avrami’s linear retrogression, based on R^2 closest value to unity and low root mean square error (RMSE: 1.4782–2.7775). The kinetic fitting quality changes in the subsequent order: Avrami > PSO > PFO. The Avrami model has value of R^2 (> 0.98).

Another kinetic model, reliant on chemical sorption, is the particle diffusion model. It entails the replacing or sharing electrons between the sorbent and metal ions (Jiang et al. 2010). It is assumed that adsorption occurs due to the flow of metal ions from the liquid to the sorbent exterior surface, ensued by ions dispersal into the pores. It is a time-consuming process that is proportional to time^{0.5} denoted as (Covelo et al. 2007):

$$q_t = k_{id} t^{0.5} + I \quad (13)$$

q_t is the amount of adsorbed ions after contact time t where $t^{0.5}$ is its square root and K_{id} ($\text{mg g}^{-1} \text{min}^{-0.5}$) is the rate constant and I is the intercept whose values provide statistics about the boundary layer’s depth, i.e., the bigger the intercept the larger the influence of that borderline layer is (Chouchane et al. 2021).

Figure 9 and Table 5 show that the diffusion represents a restraining phase in the operations on the sorbent. The increased adsorption capacity confirms the presence of mesopores, with a significant amount of sites, unlocked for the small ions. However, the linear plot of $t^{0.5}$ against q_t , fit data with good linear regression coefficients ($R^2 \approx 0.91$). It indicates the applicability of the model and the rate-monitoring step is intra-particle diffusion (Goldberg 2018).

Temperature impact and sorption thermodynamics

Figure 10 displays the influence of temperature on the adsorption process. The extreme uptake capacity was reached at 65 °C, signifying that the adsorption is an endothermic process. Most adsorption studies suggest that increasing the temperature improves the sorption process (Argun 2008; Mercado-Borrayo et al. 2020; Plaza et al. 2021). Typically, at higher temperatures, the uptake is greater due to an increase in the energetic spots of the sorbent material. At increased temperatures, the system’s energy promotes the ions’ attachment to the mineral’s surface (Arief et al. 2008). Also, the movement of the ions becomes faster due to decreasing the viscosity of the solution (Fakari and Nezamzadeh-Ejhih 2017), resulting in higher removal efficiencies (Rukayat et al. 2021).

Changes in thermodynamics parameters such as Gibb’s free energy (ΔG°), entropy (ΔS°), and enthalpy (ΔH°) (Plaza et al. 2021) were determined. ΔH° and ΔS° were computed from Van’t Hoff equation (Karmaker et al. 2019):

$$\ln K_c = \frac{\Delta S^\circ}{R} - \frac{\Delta H^\circ}{RT} \quad (14)$$

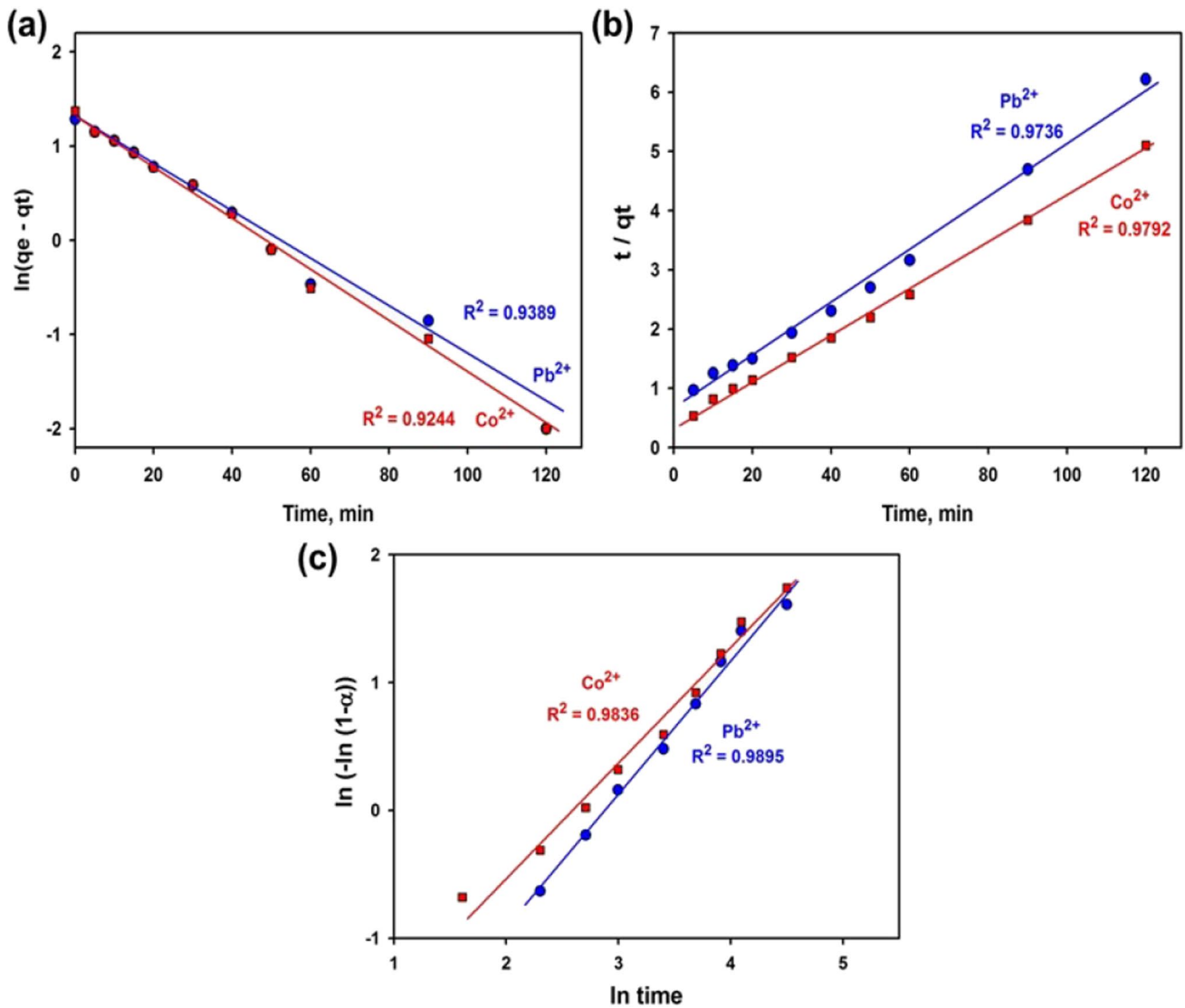


Fig. 8 Plotting results according to the three kinetics models **a** pseudo-first-order, **b** pseudo-second-order, and **c** Avrami

where $kc = F/(1 - F)$ and $F = (C_0 - C_e)/C_0$ (Adeogun et al. 2018), R is the universal gas constant, and T is the temperature in K. The relationship of $\ln kc$ versus $1/T$ (Fig. 11) gives a straight line with a slope of $-\Delta H^\circ/R$ and an intercept equals to $\Delta S^\circ/R$. The positive values of ΔH° in Table 6 specified the endothermic sorption process. Additionally, the ΔH° value $< 30 \text{ kJ mol}^{-1}$ verifies the physisorption process as shown by the Freundlich isotherm (Karmaker et al. 2019). Additionally, ΔS° was found to have positive values, suggesting a degree of unpredictability at the interface between the sorbent and adsorbate, inferring that sorption is less advantageous at lower temperatures.

ΔG° is estimated via the subsequent relation (Hoang et al. 2019):

$$\Delta G^\circ = -RT \ln K_c \tag{15}$$

Table 6 shows that the sorption is unprompted since the ΔG° has negative values. It should be pointed out here that as the temperature rose, so did the negative values of ΔG° , suggesting that sorption is more favorable at higher temperatures (Ghasemi et al. 2020; Hassan et al. 2020).

Adsorption mechanism

As revealed by isotherm studies, the adsorption process fits the Freundlich isotherm thus obeying multilayer sorption of Pb²⁺ and Co²⁺ on BFS (physical adsorption). Inner layer sorption of metal ions on BFS might be ascribed to

Table 4 Different parameters of the kinetics models

Model	Item	Pb ²⁺	Co ²⁺
1 st order	R ²	0.9389	0.9244
	K ₁	-0.0614	-0.0637
	q _{max} cal	20.4	21.6
	q _{max} exp	19.3	23.5
	RMSE	6.5114	8.3991
2 nd order	R ²	0.9736	0.9792
	K ₂	0.0032	0.0043
	q _{max} cal	22.2	25.7
	q _{max} exp	19.3	23.5
	RMSE	4.5028	4.1203
Avrami	R ²	0.9895	0.9836
	n	1.1797	1.1882
	K	0.0580	0.0759
	RMSE	1.4782	2.7775

cal. calculated, exp. experimental

the creation of metal-Si complex between the Pb²⁺/Co²⁺ ion and Si of the slag via the exchange of H⁺ ions in the circumference. Moreover, the negatively charged BFS surface (at pH 6) favors the electrostatic interaction with positive metal ions.

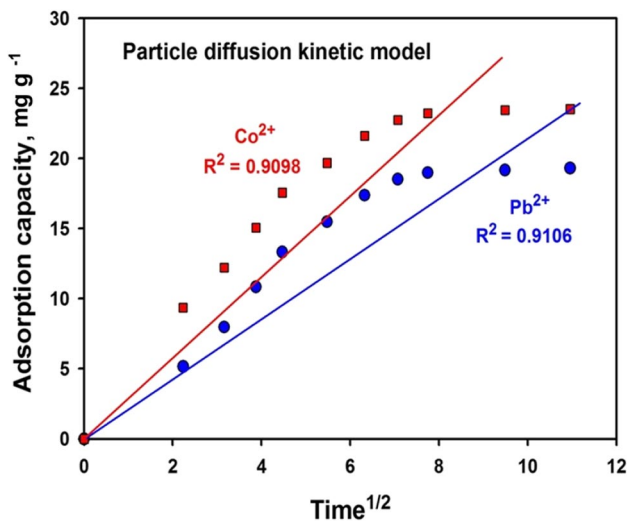


Fig. 9 Plot of particle diffusion kinetic model

Table 5 Parameters of particle diffusion model

Parameter	Pb ²⁺	Co ²⁺
linear regression coefficients (R ²)	0.9106	0.9098
Thickness of boundary layer (l)	2.8206	5.4130
Rate constant of intra-particle diffusion (K _{id})	1.8917	2.1189

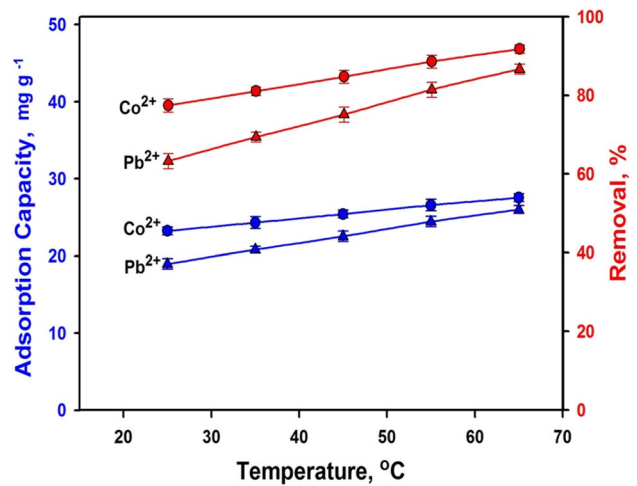
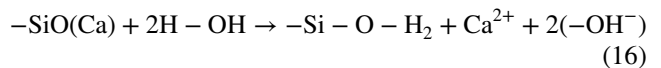


Fig. 10 Effect of temperature on the removal efficiency of Co²⁺ and Pb²⁺ ions and adsorption capacity of BFS

As a result, the electrostatic interaction between Pb²⁺/Co²⁺ ions and the groups (such as -CO₃ and -OH) on the sorbent is linked with multilayer adsorption of metal ions. Metal-sulfur complex formation via ion exchange and electrostatic interactions is thought to be a viable mechanistic mechanism for metal-ion adsorption on the BFS (Deng et al. 2020). Considering the nature and composition of the BFS, an exchange interaction of the slag with the effluent may be described as coming (Dimitrova and Mehandgiev 1998):



It can be anticipated that because of the large concentration of hydrogen ions in an acidic environment, the above

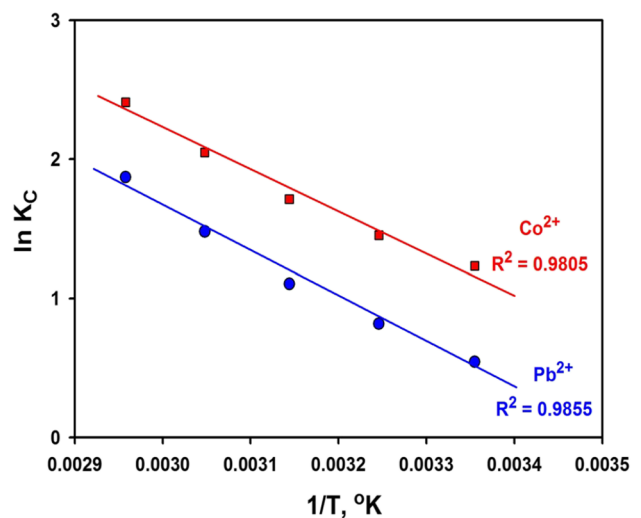


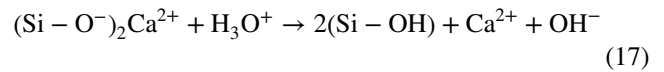
Fig. 11 Plot of lnK_c versus 1/T

Table 6 Thermodynamic parameters of Co²⁺ and Pb²⁺ ions sorption on BFS

Metal ion	Temp. (°C)	ΔG° (kJ mol ⁻¹)	ΔH° (kJ mol ⁻¹)	ΔS° (J mol ⁻¹ k ⁻¹)
(Pb ²⁺)	25	-1346	27.6	96.7
	35	-2092		
	45	-2918		
	55	-4032		
	65	-5253		
(Co ²⁺)	25	-3052	24.6	92.2
	35	-3719		
	45	-4528		
	55	-5586		
	65	-6772		

reaction should shift to the left side. Following the aforesaid approach, the basic slags had a neutralizing impact.

Undoubtedly, Ca²⁺ ions interacted with the freed H⁺ ions from the slag when the solution pH rose, confirming the occurrence of the reaction in Eq. (17) when the BFS came in contact with solutions. The BFS slag exhibited a strong ion exchange capacity, which was consistent with the sorption equilibrium. For divalent metal ions (M²⁺) in solutions, the aforementioned equation may be expressed as (Zhan et al. 2019):



The lone pair of electrons in the oxygen atoms of OH⁻ groups play an important role in the complexation between metal ions and these OH⁻ groups (Wang et al. 2021) as illustrated in the schematic diagram shown in Fig. 12.

Regeneration and desorption

The regeneration and reusability of the slag for Co²⁺ and Pb²⁺ ions removal was examined under the maximum adsorption conditions: 50 mg L⁻¹ initial ions concentration; 3.3 g L⁻¹ slag dose; pH 6; at 65 °C; and time of 60 min. Whereas the conditions for regeneration were 0.1 M HNO₃; solid/liquid ratio of 1:10; at 60 °C for 30 min contact. As revealed in Fig. S1, the adsorbed cobalt and lead ions on the slag surface could be efficaciously desorbed with efficiency exceeding 91% for the first cycle. Additionally, the removal efficiency was reduced by a few percent in the next three cycles. These results revealed that the slag could be reused repetitively to get rid of Co²⁺ and Pb²⁺ ions from discharge effluents.

It is worth noting that many laws in Egypt control wastewater reuse such as Egypt decrees no. 92/2013, and no. 208/2018 for protection of Nile River and its waterways from pollution coming from industrial activities (Egypt Decree 92/2013, Egypt

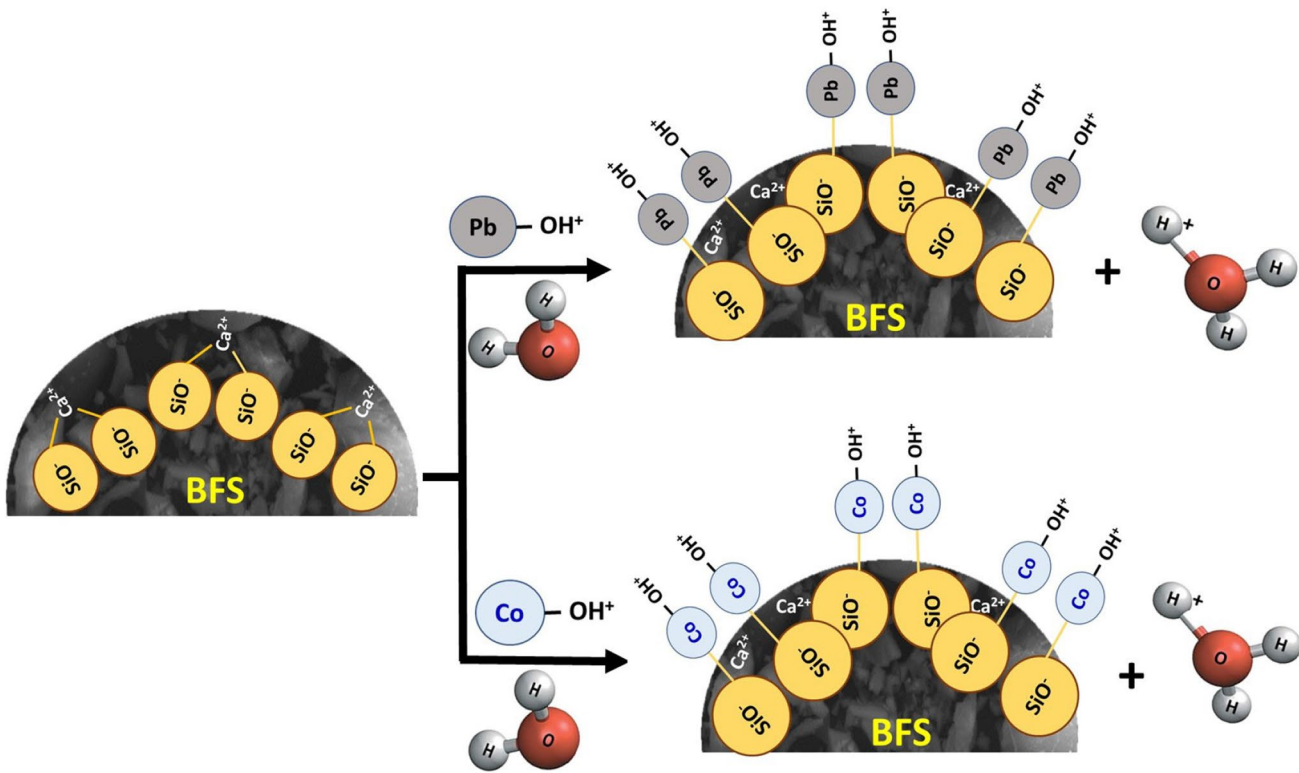


Fig. 12 Schematic illustration of Pb and Co metal ions adsorption process by BFS

decree No. 208/2018. Characteristics of the treated effluent in our study were complying with the permissible Egyptian limits for Co(II) (0.5 mg/L), Pb(II) (0.01 mg/L), and Fe (0.3 mg/L) for reclaimed water reuse standard according to these decrees.

The slag market is likely to vary, but industry efforts to promote “sustainable” materials and methods, as well as recycling in general, are likely to favor increased slag use and cost reduction. Furthermore, no chemicals were used in this study to convert BFS to adsorbent. Comparison with the other adsorbents such as activated alumina ($0.60\text{--}1.19 \times 10^3$ USD/ton), modified graphene oxide ($\sim 60 \times 10^4$ USD/ton), and zeolite ($30\text{--}120 \times 10^3$ USD/ton) (Plaza et al. 2021), the cost of BFS will surely be much lower. The versatility of the described method is also enhanced by the fact that after the treatment, a settling process can easily separate the adsorbent from the effluent, allowing the adsorbent to be reused due to its high density.

To sum up, the present study using blast furnace slag has touched on the technical merit of slags that can be used as efficient adsorbents for decontaminating waste effluents of industries. Additionally, the gained outcomes assert promisingly that the considered process may meet the requirements of using slag adsorbents at a cheap and plentiful source for large-scale production. Comparison with the other iron steel and slag adsorbents used for Pb^{2+} and Co^{2+} removal from wastewater is exhibited in Table S3 in the supplemental file.

Conclusion

Blast furnace slag (BFS) has a complex composition. Its surface charge is pH-dependent, where the isoelectric point is at pH 4.8. It was successfully used, without modification, as a sorbent of heavy metal ions. Its selectivity follows the order of $\text{Co}^{2+} > \text{Pb}^{2+}$ which is attributed to the hydration energy and charge density. The Freundlich isotherm model fits well indicating the physical nature of the sorption progression and the dimensionless separation factor (R_L) indicates its favorability. The higher adsorption amount in the first duration verified the sorption favorability on the BFS exterior surface over that in the interior pores. The particle diffusion model describes that the sorption is occurred by the ions flowing from the aqueous phase to the sorbent's exterior surface, pursued by ions dispersion into the apertures and pores. Kinetic studies carried out indicated that the Avrami kinetic model best described the adsorption mechanism. Furthermore, the thermodynamic parameters revealed that the adsorption process was endothermic and spontaneous in nature. The slag could be regenerated and reused repetitively to remove Pb^{2+} and Co^{2+} ions from effluents. In conclusion, BFS represents a comparatively effective, low-cost, and environmentally friendly adsorbent that can be applied

industrially in the field of wastewater pollution control for the purpose of Pb^{2+} and Co^{2+} ions removal.

Supplementary Information The online version contains supplementary material available at <https://doi.org/10.1007/s11356-022-19834-3>.

Author contribution S.M. Abdelbasir: planning the whole work, investigation, materials preparation and characterizations, writing—review and editing. M.A. Abdel Khalek: investigation, adsorption studies, writing—original draft.

Funding Open access funding provided by The Science, Technology & Innovation Funding Authority (STDF) in cooperation with The Egyptian Knowledge Bank (EKB).

Data availability The authors confirm that all data supporting the study's findings are included in the article.

Declarations

Ethics approval and consent to participate Not applicable.

Consent to publication All authors consent for publication.

Conflict of interest The authors declare no conflict of interest.

Open Access This article is licensed under a Creative Commons Attribution 4.0 International License, which permits use, sharing, adaptation, distribution and reproduction in any medium or format, as long as you give appropriate credit to the original author(s) and the source, provide a link to the Creative Commons licence, and indicate if changes were made. The images or other third party material in this article are included in the article's Creative Commons licence, unless indicated otherwise in a credit line to the material. If material is not included in the article's Creative Commons licence and your intended use is not permitted by statutory regulation or exceeds the permitted use, you will need to obtain permission directly from the copyright holder. To view a copy of this licence, visit <http://creativecommons.org/licenses/by/4.0/>.

References

- Abdelbasir SM, El-Shewaikh AM, El-Sheikh SM, Ali OI (2021) Novel modified chitosan nanocomposites for Co(II) ions removal from industrial wastewater. *J Water Process Eng* 41:102008. <https://doi.org/10.1016/j.jwpe.2021.102008>
- Abdelbasir SM, McCourt KM, Lee CM, Vanegas DC (2020) Waste-derived nanoparticles: synthesis approaches, environmental applications, and sustainability considerations. *Front Chem* 8:782. <https://doi.org/10.3389/FCHEM.2020.00782/BIBTEX>
- Abdel-Khalek MA, Abdel Rahman MK, Francis AA (2017) Exploring the adsorption behavior of cationic and anionic dyes on industrial waste shells of egg. *J Environ Chem Eng* 5:319–327. <https://doi.org/10.1016/j.jece.2016.11.043>
- Abdel-Khalek MA, Abdel Rahman MK, Francis AA (2020) Experimental design and desirability analysis for optimizing the bio-sorption of liquid paint-related wastes onto solid eggshell wastes. *Environ Process* 7:493–508. <https://doi.org/10.1007/s40710-020-00435-6>

- Acheampong MA, Meulepas RJW, Lens PNL (2010) Removal of heavy metals and cyanide from gold mine wastewater. *J Chem Technol Biotechnol* 85:590–613
- Adeogun AI, Ofudje EA, Idowu MA et al (2018) Biowaste-derived hydroxyapatite for effective removal of Reactive Yellow 4 dye: equilibrium, kinetic, and thermodynamic studies. *ACS Omega* 3:1991–2000. <https://doi.org/10.1021/ACSOMEGA.7B01768>
- Ahmed MJK, Ahmaruzzaman M (2016) A review on potential usage of industrial waste materials for binding heavy metal ions from aqueous solutions. *J Water Process Eng* 10:39–47
- Akhigbe L, Ouki S, Saroj D (2015) Removal of *Escherichia coli* and heavy metals from aqueous solutions using silver-modified clinoptilolite. *Desalin Water Treat* 55:777–782. <https://doi.org/10.1080/19443994.2014.929980>
- Alaif ZO, Anjum M, Kumar R et al (2019) Synthesis of CuO–GO/TiO₂ visible light photocatalyst for 2-chlorophenol degradation, pretreatment of dairy wastewater and aerobic digestion. *Appl Nanosci (Switzerland)* 9:579–591. <https://doi.org/10.1007/s13204-018-0921-7>
- Argun ME (2008) Use of clinoptilolite for the removal of nickel ions from water: kinetics and thermodynamics. *J Hazard Mater* 150:587–595. <https://doi.org/10.1016/j.jhazmat.2007.05.008>
- Arief VO, Trilestari K, Sunarso J et al (2008) Recent progress on biosorption of heavy metals from liquids using low cost biosorbents: characterization, biosorption parameters and mechanism studies. *Clean Soil Air Water* 36:937–962
- Arzate-Salgado S-Y, Morales-Pérez A-A, Solís-López M, Ramírez-Zamora R-M (2016) Evaluation of metallurgical slag as a Fenton-type photocatalyst for the degradation of an emerging pollutant: Diclofenac. *Catalysis Today* 266:126–135. <https://doi.org/10.1016/j.cattod.2015.09.026>
- Badawi AK, Zaher K (2021) Hybrid treatment system for real textile wastewater remediation based on coagulation/flocculation, adsorption and filtration processes: Performance and economic evaluation. *J Water Process Eng* 40:101963. <https://doi.org/10.1016/J.JWPE.2021.101963>
- Badawi AK, Bakhom ES, Zaher K (2021) Sustainable evaluation of using nano zero-valent iron and activated carbon for real textile effluent remediation. *Arab J Sci Eng* 46:10365–10380. <https://doi.org/10.1007/S13369-021-05349-5/FIGURES/8>
- Bazrafshan E, Mohammadi L, Ansari-Moghaddam A, Mahvi AH (2015) Heavy metals removal from aqueous environments by electrocoagulation process—a systematic review. *J Environ Health Sci Eng* 13:1–16
- Beh CL, Chuah TG, Nourouzi MN, Choong T (2012) Removal of heavy metals from steel making waste water by using electric arc furnace slag. *E-J Chem* 9:2557–2564. <https://doi.org/10.1155/2012/128275>
- Briffa J, Sinagra E, Blundell R (2020) Heavy metal pollution in the environment and their toxicological effects on humans. *Heliyon* 6:e04691
- Carvalho J, Araujo J, Castro F (2011) Alternative low-cost adsorbent for water and wastewater decontamination derived from eggshell waste: an overview. *Waste Biomass Valorization* 2:157–167
- Chen Q, Wang H, Hu E et al (2020) Efficient adsorption of uranium (VI) from aqueous solution by a novel modified steel slag adsorbent. *J Radioanal Nucl Chem* 323:73–81. <https://doi.org/10.1007/S10967-019-06848-4/FIGURES/12>
- Chen XJ, Guo YX, Cheng FQ, Song HP, Zheng N, Wang XM (2012) Application of modified coal fly ash as an adsorbent for ammonia-nitrogen wastewater treatment. In advanced materials research. *Trans Tech Publications, Ltd* 518–523:2380–2384. <https://doi.org/10.4028/www.scientific.net/amr.518-523.2380>
- Cheng M, Zeng G, Huang D et al (2017) Salicylic acid–methanol modified steel converter slag as heterogeneous Fenton-like catalyst for enhanced degradation of alachlor. *Chem Eng J* 327:686–693. <https://doi.org/10.1016/j.cej.2017.06.153>
- Chouchane T, Khireddine O, Boukari A (2021) Kinetic studies of Ni(II) ions adsorption from aqueous solutions using the blast furnace slag (BF slag). *J Eng Appl Sci* 68(1):1–18. <https://doi.org/10.1186/S44147-021-00039-3>
- Covelo EF, Vega FA, Andrade ML (2007) Simultaneous sorption and desorption of Cd, Cr, Cu, Ni, Pb, and Zn in acid soils: I. Selectivity sequences. *J Hazard Mater* 147:852–861. <https://doi.org/10.1016/J.JHAZMAT.2007.01.123>
- Decree of Minister of Water Resources and Irrigation, no. 92 for year 2013 for the Executive Regulation of, Law 48/1982 92/2013 (in Arabic). Egypt decree, 92/2013, For the Protection of the Nile River and its Waterways from Pollution
- Deng M, Wang X, Li Y et al (2020) Reduction and immobilization of Cr(VI) in aqueous solutions by blast furnace slag supported sulfidized nanoscale zerovalent iron. *Sci Total Environ* 743:140722. <https://doi.org/10.1016/J.SCITOTENV.2020.140722>
- Dimirkou A (2007) Uptake of Zn²⁺ ions by a fully iron-exchanged clinoptilolite. Case study of heavily contaminated drinking water samples. *Water Res* 41:2763–2773. <https://doi.org/10.1016/j.watres.2007.02.045>
- Dimitrova SV, Mehandgiev DR (1998) Lead removal from aqueous solutions by granulated blast-furnace slag. *Water Res* 32:3289–3292. [https://doi.org/10.1016/S0043-1354\(98\)00119-5](https://doi.org/10.1016/S0043-1354(98)00119-5)
- Egypt decree No. 208/2018 “for the protection of the Nile River and its waterways from pollution”, Decree of the Minister of Water Resources and Irrigation for the Executive Regulation of Law 48/1982, 2018 (in Arabic)
- Elboughdiri N (2020) The use of natural zeolite to remove heavy metals Cu (II), Pb (II) and Cd (II), from industrial wastewater. *Cogent Eng* 7. <https://doi.org/10.1080/23311916.2020.1782623>
- Fakari S, Nezamzadeh-Ejehieh A (2017) Synergistic effects of ion exchange and complexation processes in cysteine-modified clinoptilolite nanoparticles for removal of Cu(II) from aqueous solutions in batch and continuous flow systems. *New J Chem* 41:3811–3820. <https://doi.org/10.1039/c7nj00075h>
- Fathy MA, Abdelbasir SM, Hassan SS et al (2021) Mechanochemical activation for lead extraction from spent cathode ray tube. *J Mater Cycles Waste Manag* 23(3):1090–1101. <https://doi.org/10.1007/S10163-021-01198-4>
- Fu F, Wang Q (2011) Removal of heavy metal ions from wastewaters: a review. *J Environ Manage* 92:407–418
- Gao H, Song Z, Zhang W et al (2017) Synthesis of highly effective adsorbents with waste quenching blast furnace slag to remove Methyl Orange from aqueous solution. *J Environ Sci (China)* 53:68–77. <https://doi.org/10.1016/j.jes.2016.05.014>
- Ghasemi Z, Sourinejad I, Kazemian H et al (2020) Kinetics and thermodynamic studies of Cr(VI) adsorption using environmental friendly multifunctional zeolites synthesized from coal fly ash under mild conditions. *Chem Eng Commun* 207:808–825. <https://doi.org/10.1080/00986445.2019.1630389>
- Goldberg S (2018) Equations and models describing adsorption processes in soils. In: *Chemical Processes in Soils*. John Wiley & Sons, Ltd, pp 489–517. <https://doi.org/10.2136/sssabookser8.c10>
- Gomes HI, Funari V, Mayes WM et al (2018) Recovery of Al, Cr and V from steel slag by bioleaching: batch and column experiments. *J Environ Manage* 222:30–36. <https://doi.org/10.1016/j.jenvman.2018.05.056>
- Gupta N, Kushwaha AK, Chattopadhyaya MC (2012) Adsorptive removal of Pb²⁺, Co²⁺ and Ni²⁺ by hydroxyapatite/chitosan composite from aqueous solution. *J Taiwan Inst Chem Eng* 43:125–131. <https://doi.org/10.1016/j.jtice.2011.07.009>
- Hałas P, Kolodyńska D, Plaza A et al (2017) Modified fly ash and zeolites as an effective adsorbent for metal ions from aqueous solution. *Adsorpt Sci Technol* 35:519–533. <https://doi.org/10.1177/0263617417700420>

- Han C, Wang Z, Yang W et al (2016) Effects of pH on phosphorus removal capacities of basic oxygen furnace slag. *Ecol Eng* 89:1–6. <https://doi.org/10.1016/j.ecoleng.2016.01.004>
- Hassan ESRE, Rostom M, Farghaly FE, Abdel Khalek MA (2020) Bio-sorption for tannery effluent treatment using eggshell wastes; kinetics, isotherm and thermodynamic study. *Egypt J Pet* 29:273–278. <https://doi.org/10.1016/j.ejpe.2020.10.002>
- He J, Duan C (2016) Recovery of metallic concentrations from waste printed circuit boards via reverse floatation. *Waste Manage.* <https://doi.org/10.1016/j.wasman.2016.11.019>
- He K, Chen Y, Tang Z, Hu Y (2015) Removal of heavy metal ions from aqueous solution by zeolite synthesized from fly ash. *Environ Sci Pollut Res* 23(3):2778–2788. <https://doi.org/10.1007/S11356-015-5422-6>
- Ho YS, McKay G (1998) A comparison of chemisorption kinetic models applied to pollutant removal on various sorbents. *Process Saf Environ Prot* 76:332–340. <https://doi.org/10.1205/095758298529696>
- Hoang LP, Van HT, Nguyen LH et al (2019) Removal of Cr(vi) from aqueous solution using magnetic modified biochar derived from raw corncob. *New J Chem* 43:18663–18672. <https://doi.org/10.1039/c9nj02661d>
- Hoslett J, Ghazal H, Mohamad N, Jouhara H (2020) Removal of methylene blue from aqueous solutions by biochar prepared from the pyrolysis of mixed municipal discarded material. *Sci Total Environ* 714. <https://doi.org/10.1016/j.scitotenv.2020.136832>
- Ihsanullah AA, Al-Amer AM et al (2016) Heavy metal removal from aqueous solution by advanced carbon nanotubes: Critical review of adsorption applications. *Sep Purif Technol* 157:141–161
- Issaoui H, Sallem F, Lafaille J et al (2021) Biosorption of heavy metals from water onto phenolic foams based on tannins and lignin alkaline liquor. *Int J Environ Res* 15(2):369–381. <https://doi.org/10.1007/S41742-021-00313-5>
- Jaishankar M, Tseten T, Anbalagan N et al (2014) Toxicity, mechanism and health effects of some heavy metals. *Interdiscip Toxicol* 7:60–72
- Jiang M-q, Jin X-y, Lu XQ, Chen Z-l (2010) Adsorption of Pb(II), Cd(II), Ni(II) and Cu(II) onto natural kaolinite clay. *Desalination* 252:33–39. <https://doi.org/10.1016/j.desal.2009.11.005>
- Kanel SR, Choi H, Kim JY et al (2006) Removal of arsenic(III) from groundwater using low-cost industrial by-products—blast furnace slag. *Water Qual Res J Can* 41:130–139. <https://doi.org/10.2166/wqrj.2006.015>
- Karmaker S, Sintaha F, Saha TK (2019) Kinetics, isotherm and thermodynamic studies of the adsorption of Reactive Red 239 Dye from aqueous solution by chitosan 8B. *Adv Biol Chem* 09:1–22. <https://doi.org/10.4236/abc.2019.91001>
- Khalek MAA, Mahmoud GA, Shoukry EM et al (2019) Adsorptive removal of nitrate ions from aqueous solution using modified biodegradable-based hydrogel. *Desalin Water Treat* 155:390–401. <https://doi.org/10.5004/dwt.2019.24096>
- Khulbe KC, Matsuura T (2018) Removal of heavy metals and pollutants by membrane adsorption techniques. *Appl Water Sci* 8:19. <https://doi.org/10.1007/s13201-018-0661-6>
- Kozera-Sucharda B, Gworek B, Kondzielski I (2020) The simultaneous removal of zinc and cadmium from multicomponent aqueous solutions by their sorption onto selected natural and synthetic zeolites. *Minerals* 10:343. <https://doi.org/10.3390/min10040343>
- Le QTN, Vivas EL, Cho K (2021) Oxalated blast-furnace slag for the removal of Cobalt(II) ions from aqueous solutions. *J Ind Eng Chem* 95:57–65. <https://doi.org/10.1016/J.JIEC.2020.12.003>
- Limju X (2017) APHA standard methods for the examination of water and wastewater (23rd ed.), American Public Health Association, Washington DC
- Liu SY, Gao J, Yang YJ et al (2010) Adsorption intrinsic kinetics and isotherms of lead ions on steel slag. *J Hazard Mater* 173:558–562. <https://doi.org/10.1016/j.jhazmat.2009.08.122>
- Lopes ECN, dos Anjos FSC, Vieira EFS, Cestari AR (2003) An alternative Avrami equation to evaluate kinetic parameters of the interaction of Hg(II) with thin chitosan membranes. *J Colloid Interface Sci* 263:542–547. [https://doi.org/10.1016/S0021-9797\(03\)00326-6](https://doi.org/10.1016/S0021-9797(03)00326-6)
- Maged A, Ismael IS, Kharbish S et al (2020) Enhanced interlayer trapping of Pb(II) ions within kaolinite layers: intercalation, characterization, and sorption studies. *Environ Sci Pollut Res* 27:1870–1887. <https://doi.org/10.1007/s11356-019-06845-w>
- Mahmoud GA, Abdel Khalek MA, Shoukry EM et al (2019) Removal of phosphate ions from wastewater by treated hydrogel based on chitosan. *Egypt J Chem* 62:1537–1549. <https://doi.org/10.21608/EJCHEM.2019.9627.1646>
- Medina TJ, Arredondo SP, Corral R et al (2020) Microstructure and pb²⁺ adsorption properties of blast furnace slag and fly ash based geopolymers. *Minerals* 10:1–17. <https://doi.org/10.3390/min10090808>
- Mercado-Borraro BM, Contreras R, Sánchez A et al (2020) Optimisation of the removal conditions for heavy metals from water: a comparison between steel furnace slag and CeO₂ nanoparticles. *Arab J Chem* 13:1712–1719. <https://doi.org/10.1016/j.arabjc.2018.01.008>
- Mostafa NY, El-Hemaly SAS, Al-Wakeel EI et al (2001) Characterization and evaluation of the hydraulic activity of water-cooled slag and air-cooled slag. *Cem Concr Res* 31:899–904. [https://doi.org/10.1016/S0008-8846\(01\)00497-5](https://doi.org/10.1016/S0008-8846(01)00497-5)
- Narayanan S, Tamizhdurai P, Mangesh VL et al (2020) Recent advances in the synthesis and applications of mordenite zeolite - review. *RSC Adv* 11:250–267
- Nasuha N, Ismail S, Hameed BH (2016) Activated electric arc furnace slag as an efficient and reusable heterogeneous Fenton-like catalyst for the degradation of Reactive Black 5. *J Taiwan Inst Chem Eng* 67:235–243. <https://doi.org/10.1016/j.jtice.2016.07.023>
- Nguyen TC, Loganathan P, Nguyen TV et al (2018) Adsorptive removal of five heavy metals from water using blast furnace slag and fly ash. *Environ Sci Pollut Res* 25:20430–20438. <https://doi.org/10.1007/S11356-017-9610-4/TABLES/4>
- Ostrovskii VE (1989) Mechanism of ammonia synthesis over iron catalysts in the equilibrium region. *Theor Exp Chem* 25:193–201. <https://doi.org/10.1007/BF01135010>
- Petrakis E, Komnitsas K (2019) Effect of energy input in a ball mill on dimensional properties of grinding products. *Min Metall Explor* 36:803–816. <https://doi.org/10.1007/s42461-019-0066-6>
- Plaza L, Castellote M, Nevshupa R, Jimenez-Relinque E (2021) High-capacity adsorbents from stainless steel slag for the control of dye pollutants in water. *Environ Sci Pollut Res* 28(19):23896–23910. <https://doi.org/10.1007/S11356-020-12174-0>
- Riley AL, Mayes WM (2015) Long-term evolution of highly alkaline steel slag drainage waters. *Environ Monit Assess* 187(7):1–16. <https://doi.org/10.1007/S10661-015-4693-1>
- Rukayat OO, Usman MF, Elizabeth OM et al (2021) Kinetic adsorption of heavy metal (Copper) on rubber (*Hevea Brasiliensis*) leaf powder. *S Afr J Chem Eng* 37:74–80. <https://doi.org/10.1016/j.sajce.2021.04.004>
- Saleem J, Bin SU, Hijab M et al (2019) Production and applications of activated carbons as adsorbents from olive stones. *Biomass Convers Biorefinery* 9:775–802
- Sall ML, Diaw AKD, Gningue-Sall D et al (2020) Toxic heavy metals: impact on the environment and human health, and treatment with conducting organic polymers, a review. *Environ Sci Pollut Res* 27:29927–29942
- Sen Gupta S, Bhattacharyya KG (2014) Adsorption of metal ions by clays and inorganic solids. *RSC Adv* 4:28537–28586
- Shehab A, Abdelbasir SM, Khalek M, Soliman M, Elgemei G (2019) 'Dye removal from aqueous solution by regenerated spent bleaching earth. World academy of science, engineering and technology, open science index 153. *Int J Chem Mater Eng* 13(9):452–461
- Sundhararasu E, Tuomikoski S, Runtti H et al (2021) Alkali-activated adsorbents from slags: column adsorption and regeneration study for nickel(II) removal. *Chem Eng* 5:13. <https://doi.org/10.3390/CHEMENGINEERING5010013>
- Tsai W-T, Chen H-R (2013) Adsorption kinetics of herbicide paraquat in aqueous solution onto a low-cost adsorbent, swine-manure-derived

- biochar. *Int J Environ Sci Technol* 10:1349–1356. <https://doi.org/10.1007/s13762-012-0174-z>
- Tsutsumi T, Nishimoto S, Kameshima Y, Miyake M (2014) Hydrothermal preparation of tobermorite from blast furnace slag for Cs⁺ and Sr²⁺ sorption. *J Hazard Mater* 266:174–181. <https://doi.org/10.1016/J.JHAZMAT.2013.12.024>
- Vaghetti JCP, Lima EC, Royer B et al (2009) Pecan nutshell as biosorbent to remove Cu(II), Mn(II) and Pb(II) from aqueous solutions. *J Hazard Mater* 162:270–280. <https://doi.org/10.1016/j.jhazmat.2008.05.039>
- Visa M (2016) Synthesis and characterization of new zeolite materials obtained from fly ash for heavy metals removal in advanced wastewater treatment. *Powder Technol* 294:338–347. <https://doi.org/10.1016/j.powtec.2016.02.019>
- Wang F, Lu X, Li XY (2016) Selective removals of heavy metals (Pb²⁺, Cu²⁺, and Cd²⁺) from wastewater by gelation with alginate for effective metal recovery. *J Hazard Mater* 308:75–83. <https://doi.org/10.1016/j.jhazmat.2016.01.021>
- Wang Y, Li H, Cui S, Wei Q (2021) Adsorption behavior of lead ions from wastewater on pristine and aminopropyl-modified blast furnace slag. *Water* 13:2735. <https://doi.org/10.3390/W13192735>
- Xiong J, He Z, Mahmood Q et al (2008) Phosphate removal from solution using steel slag through magnetic separation. *J Hazard Mater* 152:211–215. <https://doi.org/10.1016/j.jhazmat.2007.06.103>
- Xue Y, Hou H, Zhu S (2009) Adsorption removal of reactive dyes from aqueous solution by modified basic oxygen furnace slag: Isotherm and kinetic study. *Chem Eng J* 147:272–279. <https://doi.org/10.1016/j.cej.2008.07.017>
- Yang L, Wen T, Wang L et al (2019) The stability of the compounds formed in the process of removal Pb(II), Cu(II) and Cd(II) by steelmaking slag in an acidic aqueous solution. *J Environ Manage* 231:41–48. <https://doi.org/10.1016/J.JENVMAN.2018.10.028>
- Yildirim IZ, Prezzi M (2011) Chemical, mineralogical, and morphological properties of steel slag. *Adv Civ Eng* 2011:463638. <https://doi.org/10.1155/2011/463638>
- Zare EN, Lakouraj MM, Masoumi M (2018) Efficient removal of pb (II) and Cd (II) from water by cross-linked poly (N-vinylpyrrolidone-co-maleic anhydride)/eggshell/Fe₃O₄ environmentally friendly nano composite. *Desalin Water Treat* 106:209–219. <https://doi.org/10.5004/dwt.2018.22104>
- Zare EN, Lakouraj MM, Ramezani A (2016) Efficient sorption of Pb(II) from an aqueous solution using a poly(aniline-co-3-aminobenzoic acid)-based magnetic core-shell nanocomposite. *New J Chem* 40:2521–2529. <https://doi.org/10.1039/c5nj02880a>
- Zhan X, Xiao L, Liang B (2019) Removal of Pb(II) from acid mine drainage with bentonite-steel slag composite particles. *Sustainability* 11:4476. <https://doi.org/10.3390/SU11164476>

Publisher's note Springer Nature remains neutral with regard to jurisdictional claims in published maps and institutional affiliations.